Pulsed ENDOR determination of the arginine location in the ferrous–NO form of neuronal NOS

ARTICLE *in* THE JOURNAL OF PHYSICAL CHEMISTRY A · JUNE 2012

Impact Factor: 2.69 · DOI: 10.1021/jp302319c · Source: PubMed

THE JOURNAL OF PHYSICAL CHEMISTRY A

Article

pubs.acs.org/JPCA

Pulsed ENDOR Determination of the Arginine Location in the Ferrous−NO Form of Neuronal NOS

Andrei V. Astashkin,[†] Bradley O. Elmore,[‡] Li Chen,[‡] Weihong Fan,[‡] J. Guy Guillemette,[§] and Changjian Feng*[,‡]

[†]Department of Chemistry and Biochemistry, University of Arizona, Tucson, Arizona 85721, United States

[‡]Department of Pharmaceutical Sciences, College of Pharmacy, University of New Mexico, Albuquerque, New Mexico 87131, United States

[§]Department of Chemistry, University of Waterloo, Waterloo, Ontario N2L 3G1, Canada

ABSTRACT: Mammalian nitric oxide synthases (NOSs) are enzymes responsible for oxidation of L-arginine (L-Arg) to nitric oxide (NO). Mechanisms of reactions at the catalytic heme site are not well understood, and it is of current interest to study structures of the heme species that activates O_2 and transforms the substrate. The NOS ferrous−NO complex is a close mimic of the obligatory ferric (hydro)peroxo intermediate in NOS catalysis. In this work, pulsed electron−nuclear double resonance (ENDOR) was used to probe the position of the L-Arg substrate at the NO•-coordinated ferrous heme center(s) in the oxygenase domain of rat neuronal NOS (nNOS). The analysis of ^{2}H and ^{15}N ENDOR spectra of samples containing d_7- or guanidino-$^{15}N_2$ labeled L-Arg has resulted in distance estimates for the nearby guanidino nitrogen and the nearby proton (deuteron) at C_δ. The L-Arg position was found to be noticeably different from that in the X-ray crystal structure of nNOS ferrous−NO complex [Li et al. *J. Biol. Inorg. Chem.* **2006**, *11*, 753−768], with the nearby guanidino nitrogen being ~0.5 Å closer to, and the nearby H_δ about 1 Å further from, the NO ligand than in the X-ray structure. The difference might be related to the structural constraints imposed on the protein by the crystal. Importantly, in spite of its closer position, the guanidino nitrogen does not form a hydrogen bond with the NO ligand, as evidenced by the absence of significant isotropic *hfi* constant for N_{g1}. This is consistent with the previous reports that it is not the L-Arg substrate itself that would most likely serve as a direct proton donor to the diatomic ligands (NO and O_2) bound to the heme.

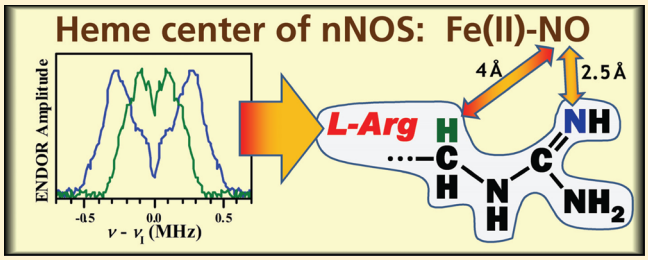

INTRODUCTION

Mammalian nitric oxide synthases (NOSs) are the enzymes responsible for NO biosynthesis.[1] There are three NOS isoforms: neuronal, endothelial, and inducible NOS (nNOS, eNOS, and iNOS, respectively). The NOS enzyme is a homodimeric flavo-hemoprotein. Each subunit of NOS contains a C-terminal electron-supplying reductase domain with binding sites for NADPH, flavin adenine dinucleotide (FAD), and flavin mononucleotide (FMN), and an N-terminal catalytic heme-containing oxygenase domain. The oxygenase and reductase domains are connected by a calmodulin (CaM)-binding region, which is tightly bound to CaM in iNOS, while reversible CaM binding is observed for nNOS and eNOS (this requires an increase in intracellular $[Ca^{2+}]$).[1,2] CaM binding to eNOS/nNOS enables electron flow from the flavin cofactors in the reductase domain to the heme[3−5] and thus activates the NO production.

NOS catalysis is a two-step process: the substrate, L-arginine (L-Arg), is first converted to *N*-hydroxy-L-arginine (NOHA), which in turn is converted to NO and citrulline.[2,6] The L-Arg substrate and a cofactor, (6*R*)-5,6,7,8-tetrahydrobiopterin (H_4B), both bind near the heme center in the oxygenase domain,[7] where the catalytic production of NO takes place. The mechanisms of the NOS heme reactions are not well understood, and it is important to study the heme species that activates O_2 and transforms the substrate.[6,8−12] In particular, it is crucial to determine structures of the obligatory ferric (hydro)peroxo intermediates that transform the substrate. Studying the O_2-coordinated heme center directly is challenging because of its high reactivity. A promising alternative strategy is to use other diatomic ligands, such as NO, that mimic the ferric (hydro)peroxo intermediate, but form more stable heme complexes.

Currently, crystal structures are only available for truncated NOS domains.[7,13−19] The separated domains of the modular NOS protein are active,[20,21] and a study of catalytic and electron transfer mechanisms by using the homologous NOS constructs represents a commonly accepted approach in the field.[1,22−25] For example, the heme-containing oxygenase domain construct, NOSoxy has been extensively used to study the oxidative pathways.[12]

Received: March 10, 2012
Revised: June 1, 2012
Published: June 5, 2012

   dx.doi.org/10.1021/jp302319c | *J. Phys. Chem. A* 2012, 116, 6731−6739

Electron paramagnetic resonance (EPR) has been used for detailed structural investigation of the NOS enzymes,[26] including the heme active center.[10,11,27−30] For ferric heme centers (of NOS and other heme proteins), however, the spin density is predominantly located on the central Fe(III), and the magnetic interactions with the nuclei of the second coordination sphere usually cannot be resolved by continuous wave EPR or even by high-resolution EPR techniques of electron−nuclear double resonance (ENDOR) and electron spin echo (ESE) envelope modulation (ESEEM) spectroscopy. It is of note that the reach of the EPR techniques can be improved if the heme center is in a high-spin Fe(III) state. Hoffman's group used ^{15}N ENDOR to determine the location of the guanidino nitrogen atom of L-Arg in a 5-coordinate high-spin ferric heme center of NOS proteins.[31,32]

Alternatively, the structure of the second coordination sphere may become more accessible for EPR if the ferrous heme center is coordinated by NO. In this case, most of the spin density in the complex is located on the NO ligand,[33−36] and the observation point is shifted by about 2 Å from Fe. The axial NO ligand is thus a potentially useful ENDOR/ESEEM probe of the NOS heme active site capable of reporting about the molecular environment on the distal side of the heme, in particular, about the interactions with the substrate and water molecules. The NOS ferrous−NO complex is also a close mimic of the obligatory ferric (hydro)peroxo intermediate in NOS catalysis. Moreover, the facts that the NO complex has intrinsic biological significance in NOS catalysis[37] and that the H-bonding capability of NO is similar to that of the dioxygen ligand make the NO-coordinated ferrous heme center of NOS an especially interesting object for EPR investigation. The main purpose of such an investigation is to obtain information about key structural components, including the positioning of the substrate molecule and the H-bonds to the substrate and active site water, and to study the changes of these parameters as a function of various regulatory elements,[1,22] in order to improve the understanding of the structure−function relationship for the reactions at the NOS heme active site. The H-bonding information is of particular importance because increasing evidence indicates that the two NOS reaction steps are distinguished by an H-bonding network near the substrates (i.e., L-Arg or NOHA) in the ferric−peroxo species.[10,12]

In this work, pulsed ENDOR was used to probe the position of the L-Arg substrate at the NO-coordinated ferrous heme active site of the oxygenase domain construct of nNOS (nNOSoxy). This specific system was chosen because the available X-ray single crystal structural data on the NO complexes of nNOSoxy protein[38] provide a reference for comparison with the ENDOR results. In particular, we intended to conclusively determine the presence or absence of an H-bond between the guanidino nitrogen of L-Arg and the NO ligand; the absence of such H-bond was inferred from the X-ray structure.[38]

In order to separate the spectroscopic signatures of the magnetic nuclei belonging to L-Arg, two kinds of isotopically labeled samples were used, with L-Arg being deuterated at all of the carbon positions (Arg-d_7) and ^{15}N-labeled at guanidino nitrogen positions (Arg-$^{15}N_g$). The latter labeling allows one to access the position of the substrate business end. As a result of our investigation, the position of the L-Arg substrate at the NO-coordinated ferrous heme center in frozen solution was found to be different from that in a single crystal, with the closest guanidino nitrogen being about 0.5 Å closer to the NO ligand than in the X-ray structure. In spite of the shorter distance, no evidence of a hydrogen bond between the NO ligand and the guanidino nitrogen of the L-Arg molecule was found.

MATERIALS AND METHODS

EPR Sample Preparation. Rat nNOSoxy construct, in which only the heme-containing oxygenase domain is present, was expressed and purified as reported earlier.[39−41] The EPR samples were prepared in a septum sealed quartz cuvette (Starna Cells, 9/Q/10-GL14-S). Three hundred microliters of 500 μM nNOSoxy was added into the cuvette; buffer, 100 mM bis-tris-propane, 200 mM NaCl, 1 mM DTT, 10 μM H_4B, 10% glycerol, pH 7.4. The protein solution was deoxygenated with three cycles of vacuum pump and purging (with dioxygen-scrubbed argon gas). NO gas was introduced into the headspace until complete disappearance of the high spin ferric heme band at 650 nm, indicative of the formation of the ferric−NO adduct. The sample was then completely reduced with an excess amount of freshly prepared dithionite solution. Solid L-Arg HCl was added to a final concentration of 10 mM; the change in pH of the sample was negligible. A ∼45 μL sample was then transferred into an EPR tube and rapidly frozen in a pentane and liquid nitrogen slurry. Three types of samples were prepared in the H_2O buffer, with d_7- or guanidino-$^{15}N_2$ labeled L-Arg HCl (denoted Arg-d_7 and Arg-$^{15}N_g$, respectively; 98%, obtained from Cambridge Isotope Laboratories Inc.), or L-Arg having natural abundance of the isotopes (denoted Arg-NA).

Pulsed EPR Experiments. The experiments were performed on a homemade K_a-band (26−40 GHz) pulsed EPR spectrometer.[42] The measurement temperature was 15 K. The detailed experimental conditions are described in the figure captions. All of the samples contained 10 mM L-Arg.

RESULTS AND DISCUSSION

Structural Background. The structural and electronic−structural parameters essential for interpreting the pulsed ENDOR spectra obtained in this work are the orientation of the g-frame with respect to the molecular frame and the spin density distribution in the Fe−N−O fragment. For NO-coordinated ferrous heme centers, the orientation of the g-tensor with respect to the molecular coordinate frame was established both by combined X-ray and EPR studies of single crystals and by DFT calculations.[33−35,43] The results depend on the coordination state (5- or 6-coordinate) of the heme and on the type of the axial ligand trans to NO. The heme center of NO-bound nNOS is 6-coordinate,[38] with the protein-derived axial ligand being a cysteine residue, the same as in P450. Interestingly, the EPR spectrum of the Fe(II)−NO center of NOS[44] (also see below) is not only similar to that of P450[45,46] but is also similar to the spectra of the imidazole bound ferrous−NO heme centers.[43,45,47] This was explained by the similar strengths of the axial interactions in the Fe−N bond of the imidazole complex and Fe−S bond in the complex with cysteine.[33] The spectroscopic and DFT results for such a center[33−35,43,48] predict the axis of the largest principal g-value, g_Z, to be parallel to the heme plane and perpendicular to the Fe−N−O plane. The axis of the intermediate principal g-value, g_Y, is approximately perpendicular to the direction of the NO bond, while the axis of the smallest principal g-value, g_X, is approximately parallel to the NO bond.

The spin density distribution for an imidazole-coordinated ferrous NO heme center was calculated in several

works.[33−35,43,49] The predicted spin densities on Fe (ρ_{Fe}) and on the NO ligand (ρ_{NO}) varied from (ρ_{Fe}, ρ_{NO}) ≈ (0.65, 0.35) to (0.2, 0.8). The DFT calculation for the $-SCH_3$-coordinated ferrous NO center (that was supposed to approximately model the cysteine-coordinated heme of P450 or NOS) has resulted in (ρ_{Fe}, ρ_{NO}) ≈ (−0.2, 1.2).[34] The ratio of spin densities on the oxygen and nitrogen atoms of the NO ligand (ρ_O and ρ_N, respectively) is predicted to be $\rho_O/\rho_N \approx 0.6$.[36]

Given a large variability of the calculation results for the imidazole-coordinated center and a rather extreme nature of the spin density distribution predicted for the $-SCH_3$-coordinated model (especially so, given the similarity of the experimental EPR spectra between the imidazole- and cysteine-bound species), we will use the intermediate distribution, (ρ_{Fe}, ρ_{NO}) ≈ (0.2, 0.8),[33−35] as a starting point in the analysis of our experimental ENDOR spectra. The distributions with smaller or larger ρ_{NO} (within the limits obtained from the DFT calculations) will also be considered and evaluated from the viewpoint of reasonability of the structural information obtained from the ENDOR data using these distributions.

The structure of the NO-coordinated ferrous heme centers of homodimeric nNOSoxy in the presence of L-Arg was obtained by X-ray crystallography.[38] It was found that, while the overall structures of the two heme centers (A and B), including the position of the substrate L-Arg, are similar, the orientations of the NO ligand differ by about 90° (Figure 1). Taking into account the relationship between the orientation of the NO ligand and that of the g-frame axes (see above), one can conclude that the angular positions of the L-Arg protons and nitrogens with respect to the g-frame for these two sites are different. The distances of hydrogens and nitrogens of L-Arg from the main centers of spin density are also slightly different, which may potentially lead to different *hfi* for the two heme sites.

Table 1 shows the distances of hydrogens and guanidino nitrogens of L-Arg from the nitrogen of the NO ligand (denoted $N_{(NO)}$) at the two nNOS heme sites, which were obtained from the X-ray crystal structure.[38] The positions of hydrogens were calculated from the X-ray coordinates of the adjacent carbons by assuming the sp^3 hybridization for these carbons and using the CH bond length of 1.09 Å. The guanidino nitrogens are at the distances of about 3 Å (N_{g1}) and 4.3 Å (N_{g2}). The closest hydrogen, one of those at C_δ (numbered $H_{\delta 2}$ in Table 1), is also at about 3 Å from $N_{(NO)}$, with other hydrogens being significantly further away (from 4.4 to ∼8 Å). The two closest nuclei, N_{g1} and $H_{\delta 2}$ ($D_{\delta 2}$ for Arg-d_7), are mostly responsible for the appearance and the outermost features of the Mims ENDOR spectra recorded in this work.

Experimental Spectra. Figure 2 shows the field sweep ESE spectrum of Fe(II)−NO heme center of nNOS. The principal g-values determined from the turning points of this spectrum are (g_X, g_Y, g_Z) = (1.969, 2.004, 2.084). The intermediate turning point exhibits a resolved triplet splitting of ∼2.1 mT due to the ^{14}N *hfi* of the coordinated NO. Overall, the spectrum is typical for a 6-coordinate Fe(II)−NO heme center of nNOS[44] and is similar to the spectra of Fe(II)−NO complexes of P450 and Fe(II)−NO heme centers coordinated by histidine (imidazole).[45]

To specifically access the structural information about the L-Arg substrate using pulsed ENDOR spectroscopy, two types of isotope-enriched L-Arg were used: Arg-d_7 (uniformly labeled at all carbon positions) and Arg-$^{15}N_g$, with guanidino nitrogens being ^{15}N. Given the scale of distances between the closest ^2H

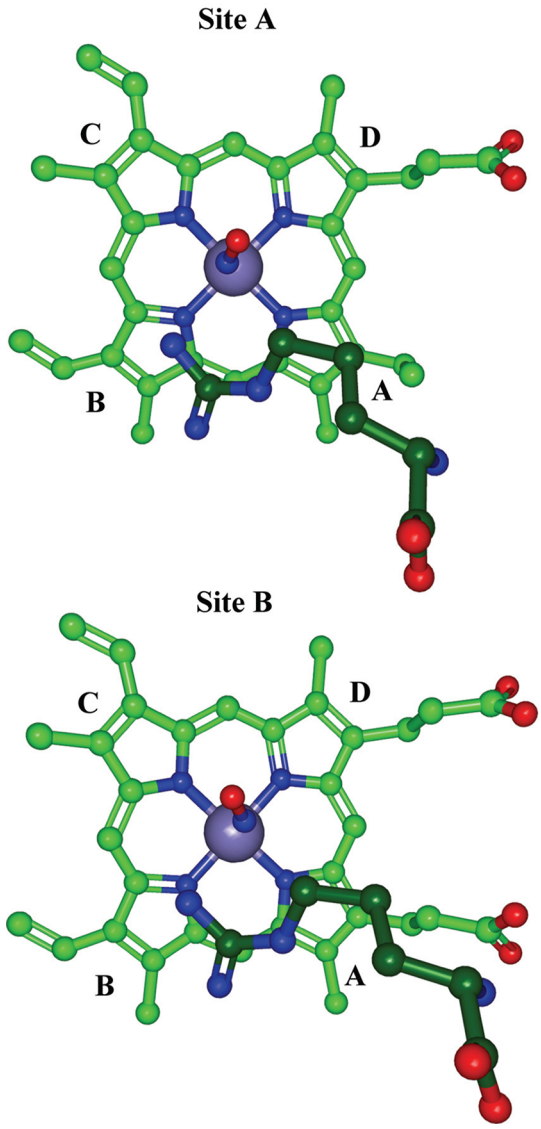

Figure 1. Relative arrangement of the NO-coordinated heme and the L-Arg substrate for two heme sites (A and B) of the dimeric oxygenase domain of nNOS as obtained by X-ray crystallography (PDB code: 2G6K).[38] The heme center is in the ferrous state. L-Arg carbons are rendered in a darker shade of green. Note the different orientations of the NO ligand in the two heme sites: the NO in chain A is turned toward the pyrrole ring D, while in chain B, it is turned toward the pyrrole ring C.

or ^{15}N of L-Arg and the NO ligand (∼3 Å), the expected anisotropic *hfi* should be on the order of 1 MHz or less. Therefore, we used the Mims ENDOR technique with a fairly large time interval between the first and second microwave (mw) pulses, τ, of 500 ns. The resulting ^2H and ^{15}N spectra were obtained as differences between the normalized (by the ESE amplitude without radio frequency, RF) Mims ENDOR spectra of isotopically labeled and unlabeled samples.

Figures 3 and 4 show, respectively, the ^2H and ^{15}N Mims ENDOR spectra taken at several positions across the EPR spectrum of the Fe(II)−NO heme center of nNOS, as indicated by arrows in Figure 2. Preliminary examination of these spectra reveals that they are in qualitative disagreement with the X-ray data. Specifically, the largest splitting observed in the ^2H ENDOR spectra is about 0.6 MHz, while in the ^{15}N

dx.doi.org/10.1021/jp302319c | J. Phys. Chem. A 2012, 116, 6731−6739

Table 1. Structural and Spectroscopic Data on Selected Atoms of L-Arg Substrate at the Heme Sites A and B of nNOS (Figure 1) Derived from the X-ray Crystallographic Coordinates[a] (PDB code: 2G6K)[38]

	site A				site B			
L-Arg atom	R (Å)	$T_{\|\|}$ (MHz)	θ_h, φ_h	θ_q, φ_q	R (Å)	$T_{\|\|}$ (MHz)	θ_h, φ_h	θ_q, φ_q
H_{α}	7.97	0.048	37°, 153°	85°, −147°	7.75	0.048	89°, 106°	37°, 166°
$H_{\beta 1}$	6.79	0.078	51°, 139°	95°, 40°	6.26	0.078	103°, 116°	102°, 184°
$H_{\beta 2}$	6.28	0.092	43°, 121°	115°, 153°	6.67	0.09	111°, 102°	148°, −13°
$H_{\gamma 1}$	5.4	0.16	45°, 162°	103°, 149°	4.88	0.16	84°, 113°	40°, 182°
$H_{\gamma 2}$	5.1	0.18	27°, 153°	95°, −62°	5.22	0.18	89°, 95°	69°, 10°
$H_{\delta 1}$	4.38	0.3	61°, 132°	121°, 133°	4.4	0.28	119°, 132°	117°, 187°
$H_{\delta 2}$	3.06	0.94	43°, 144°	122°, −80°	2.98	0.88	96°, 112°	46°, −82°
N_{g1}	2.97	−0.48	79°, 89°		3.07	−0.48	25°, 56°	
N_{g2}	4.37	−0.16	60°, 73°		4.27	−0.17	33°, 72°	

[a]The distances, R, are between the given atom and $N_{(NO)}$. The large component of the anisotropic *hfi* tensor, $T_{||}$, is estimated using a 3-point spin density distribution with (ρ_{Fe}, ρ_N, ρ_O) = (0.2, 0.5, 0.3). The orientation of the $T_{||}$ *hfi* axis with respect to the g-frame is given by the polar and azimuthal angles, θ_h and φ_h, respectively. The ^{2}H *nqi* axis orientation is given by the polar and azimuthal angles θ_q and φ_q. This axis is parallel to the corresponding C−D bond.

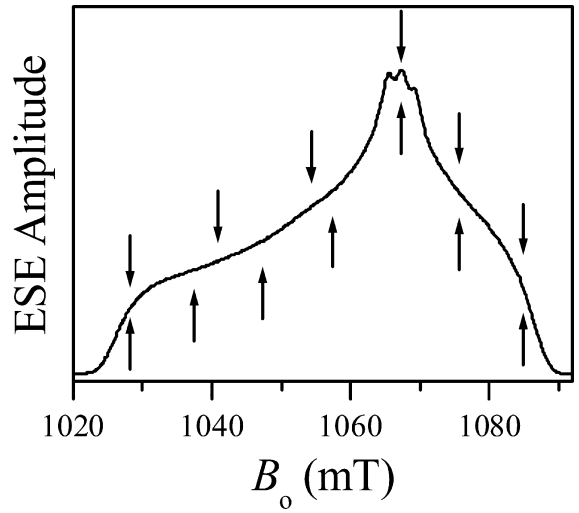

Figure 2. Two-pulse ESE field sweep spectrum of Fe(II)−NO nNOSoxy. Experimental conditions: ν_{mw} = 29.932 GHz; mw pulses, 15 and 22 ns; time interval between the mw pulses, τ = 200 ns; temperature, 15 K. The arrows pointing up and down indicate the EPR positions used for ^{2}H and ^{15}N Mims ENDOR measurements, respectively.

ENDOR spectra, it is about 1 MHz. However, the large component of the anisotropic *hfi* tensor, $T_{||}$, corresponding to the distance of 3 Å, is about 0.9 MHz for ^{2}H (i.e., ∼50% larger than the observed maximum splitting) and 0.6 MHz for ^{15}N (i.e., ∼50% smaller than the maximum splitting). This point will be demonstrated in more detail in the following section. Because of this discrepancy, it would be appropriate to analyze the dependence of the ENDOR splittings on the EPR position to estimate the distance to the deuterons and guanidino nitrogens of L-Arg and the orientations of the corresponding radius vectors with respect to the g-frame. Such an approach, however, meets a complication related to the fact that the spectra from each of the heme sites are contributed to by seven nonequivalent deuterons or two nonequivalent nitrogens. In addition, the potential nonequivalence of the heme sites as observed by the X-ray crystallography[38] will further complicate the spectra. Although, in most cases, the outermost spectral features are due to the closest nuclei ($D_{\delta 2}$ and $^{15}N_{g1}$), in some of the orientation-selective spectra with small ENDOR splittings, this may not be the case.

In order to simplify the interpretation of the spectra, it is convenient to obtain the so-called field-integrated (FI) ENDOR spectra.[50,51] They are obtained as weighted sums of the normalized (by the ESE amplitude without RF) orientation-selective spectra aligned at the Zeeman frequency of the nucleus of interest (^{2}H or ^{15}N), with the statistical weights given by the relative amplitudes of the ESE signal at the corresponding measurement positions. The FI spectra represent an approximation of the spectra that would be obtained in the orientationally nonselective situation (in this case, for the hypothetical situation of isotropic g-factor of Fe(II)−NO center). The FI ENDOR spectra obtained in such a way for ^{2}H and ^{15}N are shown by dashed lines in Figures 5 and 6, respectively.

Simulated Pulsed ENDOR Spectra. As a first step of our analysis, we calculated the FI Mims ENDOR spectra using the structural information provided by the X-ray crystallography.[38] For this, the anisotropic *hfi* tensors of the deuterons and guanidino nitrogens of L-Arg were estimated using the 3-point spin density distribution model with (ρ_{Fe}, ρ_N, ρ_O) = (0.2, 0.5, 0.3), as discussed above. All of the estimated *hfi* tensors are approximately axial (the rhombicity is <20% even for the closest nucleus, N_{g1}), and we therefore used axial tensors in our calculations. Table 1 shows the large anisotropic *hfi* tensor components, $T_{||}$, and the orientations of the corresponding principal axes for all of the deuterons and guanidino nitrogens of the substrate L-Arg in the two heme sites (Figure 1). One can see that, while the anisotropic *hfi* tensors for both sites are similar, the orientations of the tensor axes are very different.

For deuterons, one also has to consider the nuclear quadrupole interaction (*nqi*). The quadrupole coupling constant for the deutrons bound to sp^3-hybridized carbons is approximately equal to e^2Qq/h = 0.15 MHz.[52,53] The *nqi* tensor is with good accuracy axial, with the main axis being parallel to the C−D bond. The orientations of the *nqi* axes of the L-Arg deuterons for the two heme sites are shown in Table 1.

Solid lines in Figures 5 and 6 show the ^{2}H and ^{15}N FI Mims ENDOR spectra calculated using the parameters of Table 1 for both heme sites (panels a and b in each figure correspond to sites A and B, respectively). The spectra calculated for both sites are nearly identical. The main peaks with the splitting of ∼0.55 MHz, as well as the shoulders with the splitting of ∼1

dx.doi.org/10.1021/jp302319c | J. Phys. Chem. A 2012, 116, 6731−6739

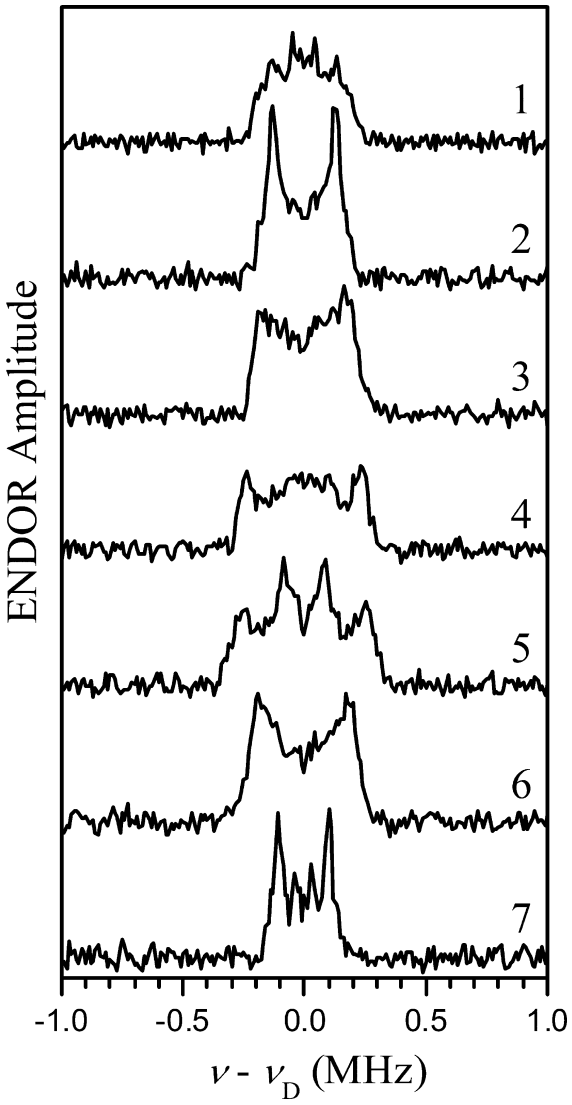

Figure 3. ^{2}H Mims ENDOR spectra of Fe(II)−NO nNOSoxy obtained at the EPR positions indicated in Figure 2 (arrows pointing up). The spectra shown represent the differences between the normalized (by the ESE amplitude without RF) spectra obtained for samples with Arg-D and Arg-NA. Traces 1 through 7 correspond to B_o = 1028.3, 1037.4, 1047.4, 1057.4, 1067.4, 1075.9, and 1084.4 mT. Other experimental conditions: ν_{mw} = 29.932 GHz; mw pulses, 3 × 12 ns; time interval between the 1st and 2nd mw pulses, τ = 500 ns; time interval between the 2nd and 3rd mw pulses, T = 60 μs; RF pulse duration, 55 μs; temperature, 15 K.

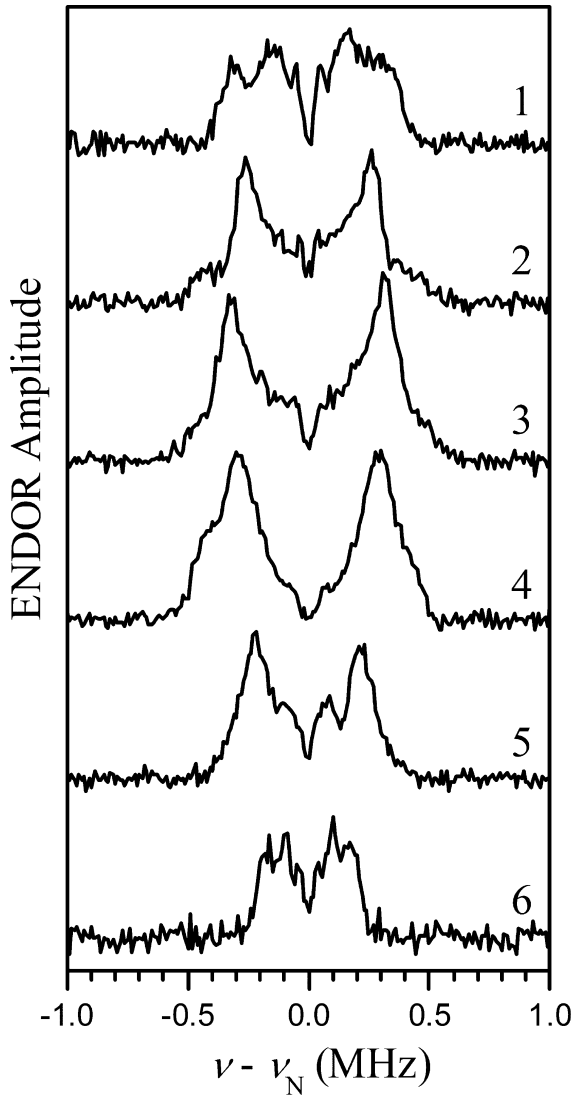

Figure 4. ^{15}N Mims ENDOR spectra of Fe(II)−NO nNOSoxy obtained at the EPR positions indicated in Figure 2 (arrows pointing down). The spectra shown represent the differences between the normalized (by the ESE amplitude without RF) spectra obtained for samples with Arg-^{15}N and Arg-NA. Traces 1 through 6 correspond to B_o = 1028.3, 1041.3, 1054.4, 1067.4, 1075.9, and 1084.4 mT. Other experimental conditions: ν_{mw} = 29.932 GHz; mw pulses, 3 × 12 ns; time interval between the 1st and 2nd mw pulses, τ = 500 ns; time interval between the 2nd and 3rd mw pulses, T = 60 μs; RF pulse duration, 55 μs; temperature, 15 K.

MHz in the calculated spectra of Figure 5, originate from $D_{\delta 2}$. As expected from the brief discussion in the previous section, the comparison with the experimental ^{2}H FI ENDOR spectrum (dashed line) shows that the splitting between the peaks in the calculated spectra, as well as their overall width, are nearly twice greater than the corresponding parameters of the experimental spectrum. For guanidino nitrogens, the situation is opposite. The splitting between the main peaks in the calculated spectra (Figure 6, solid lines) is equal to 0.24 MHz, and it is about twice smaller than the splitting between the peaks in the experimental spectrum (dashed line in Figure 6).

The first possibility to explain such a dramatic difference between the experimental and calculated ENDOR spectra is to assume that the spin density distribution in the Fe−N−O fragment is significantly different from that predicted by DFT. To test this, trial calculations of anisotropic *hfi* tensors of $D_{\delta 2}$ and N_{g1} were performed for various models of spin density distribution over the Fe−N−O fragment. In these calculations, the L-Arg positions with respect to the heme centers A and B were set to be the same as in the X-ray crystal structure.[38] These calculations have shown that it is impossible to simultaneously obtain the anisotropic *hfi* constants for $D_{\delta 2}$ and N_{g1} that would explain the experimental ENDOR splittings. Moreover, the largest possible anisotropic *hfi* constant for N_{g1}, $T_{\|}$ = −0.68 MHz, is obtained for completely unrealistic (ρ_{Fe}, ρ_{N}, ρ_{O}) = (0, 0, 1), and it is still about 30% smaller than the largest splitting observed in the ^{15}N ENDOR spectra. We thus conclude that the position of L-Arg with respect to the Fe(II)−NO heme in frozen solution is noticeably different from that in single crystal, with N_{g1} being closer to the

dx.doi.org/10.1021/jp302319c | J. Phys. Chem. A 2012, 116, 6731−6739

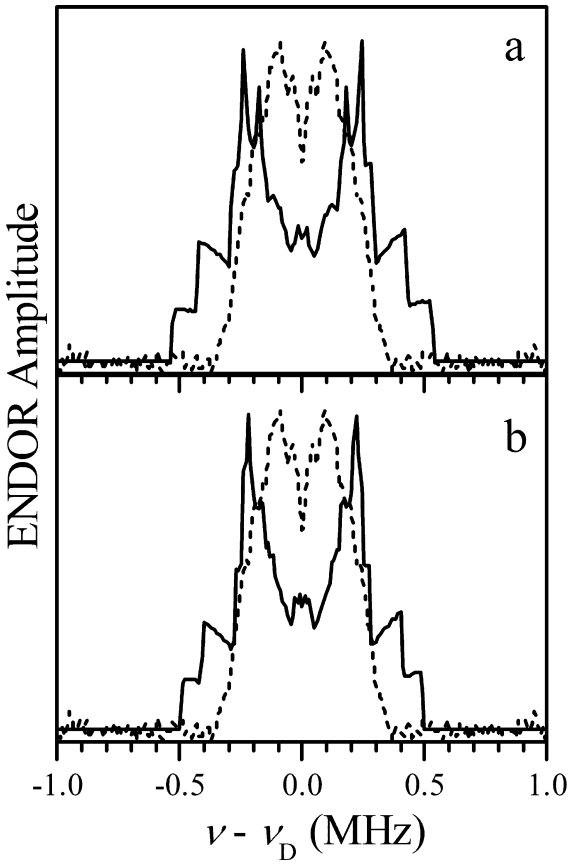

Figure 5. Comparison of the experimental field-integrated ^{2}H Mims ENDOR spectrum (dashed trace in each panel) with the simulated ^{2}H Mims ENDOR spectra (solid lines) calculated using the *hfi* and *nqi* parameters based on the X-ray crystallographic data for heme sites A (panel a) and B (panel b). The simulation parameters for each of the L-Arg deuterons are shown in Table 1, and the simulated spectra correspond to the situation of complete orientational disorder.

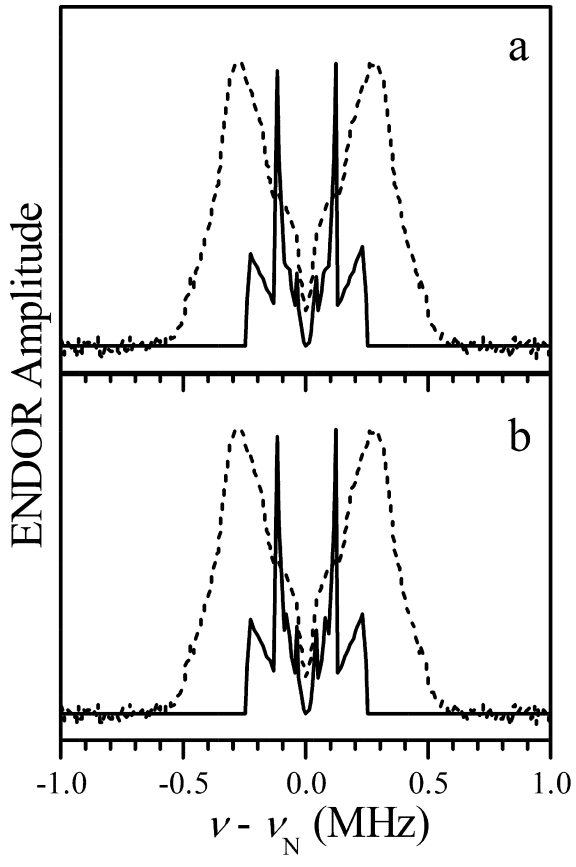

Figure 6. Comparison of the experimental field-integrated ^{15}N Mims ENDOR spectrum (dashed trace in each panel) with the simulated ^{15}N Mims ENDOR spectra (solid lines) calculated using the *hfi* parameters based on the X-ray crystallographic data for heme sites A (panel a) and B (panel b). The *hfi* parameters of the guanidino nitrogens of L-Arg are shown in Table 1, and the simulated spectra correspond to the situation of complete orientational disorder.

NO ligand, and $D_{\delta 2}$ further from NO, than in the X-ray structure.[38] We will consider the structural information in more detail after accurately estimating the anisotropic *hfi* tensors from numerical simulations of the experimental FI ENDOR spectra.

In the numerical simulations, it was assumed that the prominent outer features in the experimental spectra are mostly determined by the closest deuteron ($D_{\delta 2}$) or nitrogen (N_{g1}). For the ^{2}H ENDOR simulations, there are two variable parameters: the anisotropic *hfi* constant, $T_{\|}$, and the angle θ_{hq} between the axes of *hfi* and *nqi*. The angle θ_{hq} was varied from 0° to 90° in 15° steps, and for each θ_{hq}, the anisotropic *hfi* was selected in such a way as to fit the splitting between maxima of the experimental ^{2}H FI Mims ENDOR spectrum. The best approximations to the experimental spectrum were obtained for θ_{hq} = 30° and $T_{\|}$ = 0.36 MHz and for θ_{hq} = 90° and $T_{\|}$ = 0.38 MHz. The spectra simulated with these parameters are shown in Figure 7. Calculations using the 3-center spin density distribution with (ρ_{Fe}, ρ_{N}, ρ_{O}) = (0.2, 0.5, 0.3) result in $T_{\|}$ = 0.37 ± 0.1 MHz for R_{DN} = 3.71 − 4.45 Å (where R_{DN} is the distance between $D_{\delta 2}$ and $N_{(NO)}$), depending on the angle θ_{D} = ∠($D_{\delta 2}$−$N_{(NO)}$−$O_{(NO)}$): for θ_{D} = 0°, R_{DN} is the longest, 4.45 Å, while for θ_{D} → 90°, shorter R_{DN} is obtained. Thus, this deuteron (proton) is about 1 Å further from the NO ligand than in the X-ray crystal structure.

Let us now consider the ^{15}N ENDOR spectra. In the X-ray study,[38] it was noted that, while the distance of ∼3 Å between N_{g1} and $O_{(NO)}$ is suitable for the hydrogen bonding, such a H-bond can be excluded on the grounds of nonoptimal geometry. Our ENDOR results indicate that, in frozen solutions, the distance between N_{g1} and the NO ligand is even closer than in the crystal structure (see above), which again raises the possibility of forming the hydrogen bond. In order to address this question, one has to take into account that the H-bonding has to result in noticeable isotropic *hfi* of N_{g1}. For example, the anion radical of the first acceptor quinone in photosystem II, Q_{A}, is H-bonded to two nitrogen-containing species (imidazole moiety of histidine and a peptide nitrogen).[54,55] The isotropic *hfi* constants, a_{N}, for the H-bonded nitrogens ^{14}N are on the order of 1−2 MHz (1.5−3 MHz for ^{15}N). The spin populations of the quinone oxygens are ∼0.2−0.25,[56] quite comparable with the predicted spin population of $O_{(NO)}$ in this work, and therefore, we would expect similar a_{N} for N_{g1} (if H-bonded).

Because of the possibility of H-bonding, the ^{15}N ENDOR simulations have included a generally nonzero isotropic *hfi* constant. It was found that the largest possible *hfi* constant is obtained if the anisotropic *hfi* tensor is assumed to be axial: a_{N} = 0.08 MHz, $T_{\|}$ = −1 MHz; see trace 2 in Figure 8. However, the simulations with rhombic anisotropic *hfi* tensors resulted in smaller a_{N}. For example, trace 3 in Figure 8 shows the spectrum

dx.doi.org/10.1021/jp302319c | J. Phys. Chem. A 2012, 116, 6731−6739

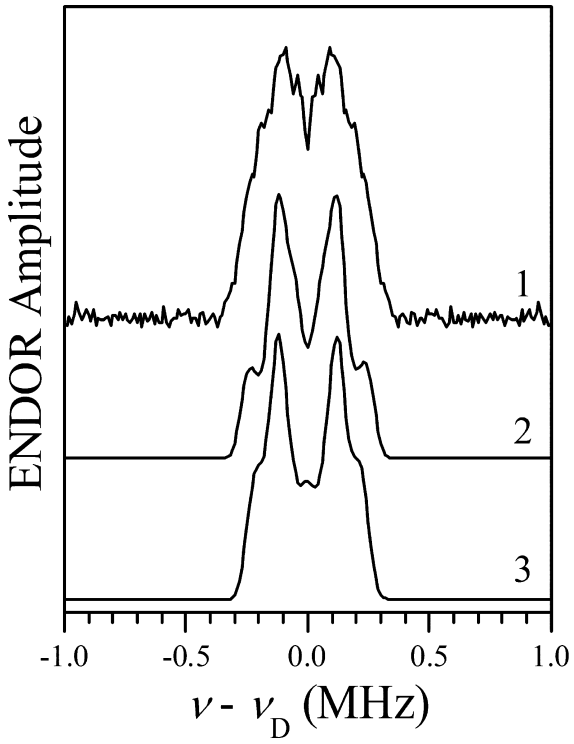

Figure 7. Experimental field-integrated (trace 1) and simulated (traces 2 and 3) ^{2}H Mims ENDOR spectra. The simulations are performed for the situation of complete orientational disorder. Simulation parameters for trace 2: $\langle a_{iso}\rangle$ = 0 MHz (where $\langle a_{iso}\rangle$ is the central value of a_{iso}); $T_{\|}$ = 0.36 MHz; e^2Qq/h = 0.15 MHz; θ_{hq} = 30°. Simulation parameters for trace 3: $\langle a_{iso}\rangle$ = 0 MHz; $T_{\|}$ = 0.38 MHz; e^2Qq/h = 0.15 MHz; θ_{hq} = 90°. Intrinsic line width is modeled by the Gaussian distribution of a_{iso} with the width between the maximum slope points of 0.1 MHz.

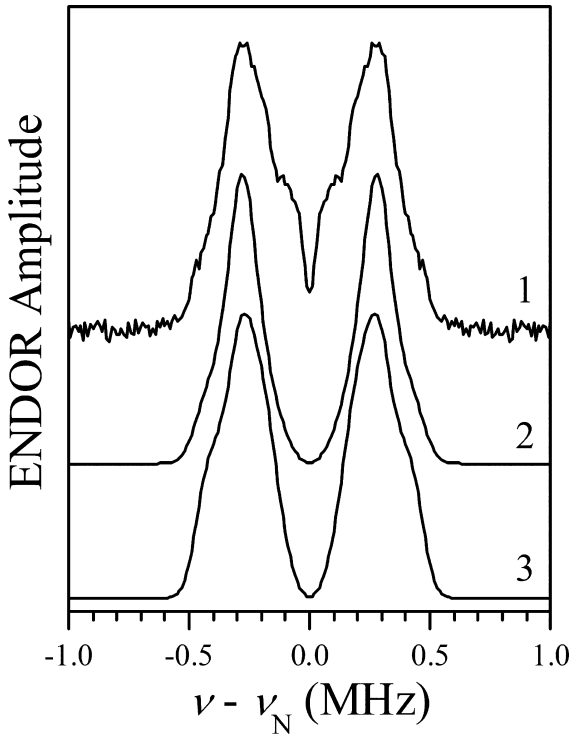

Figure 8. Experimental field-integrated (trace 1) and simulated (traces 2 and 3) ^{15}N Mims ENDOR spectra. The simulations are performed for the situation of complete orientational disorder. Simulation parameters for trace 2: $\langle a_{iso}\rangle$ = 0.08 MHz; $T_{\|}$ = −1 MHz. Simulation parameters for trace 3: $\langle a_{iso}\rangle$ = 0 MHz; (T_{11}, T_{22}, T_{33}) = (0.63, 0.3, −0.93) MHz. Intrinsic line width is modeled by the Gaussian distribution of a_{iso} with the width between the maximum slope points of 0.2 MHz (trace 2) or 0.17 MHz (trace 3).

simulated for (T_{11}, T_{22}, T_{33}) = (0.63, 0.3, −0.93) MHz and a_N = 0. In either case, the absence of significant isotropic *hfi* constant for N_{g1} suggests the lack of H-bonding between the NO ligand and the guanidino nitrogen of Arg.

The calculations for (ρ_{Fe}, ρ_N, ρ_O) = (0.2, 0.5, 0.3) result in the $T_{\|}$ component of the anisotropic *hfi* tensor between −0.9 and −1 MHz for the distances between N_{g1} and $N_{(NO)}$, R_{NgN}, in the range from 2.25 Å to 3.1 Å, depending on the angle θ_N = $\angle(N_{g1}{-}N_{(NO)}{-}O_{(NO)})$. The longest distance, R_{NgN} = 3.1 Å, corresponds to θ_N = 0°. With this arrangement, however, the distance between N_{g1} and $O_{(NO)}$ is only about 1.95 Å. Thus, regardless of θ_N, the distance between N_{g1} and the atoms of the NO ligand should be under 2.3 Å. This distance is significantly shorter than the sum of the van der Waals radii of N and O (∼3 Å), although it is still much longer than the N−N or N−O bond length (∼1.4−1.45 Å). Assuming a greater spin density on the NO ligand results in a longer distance between N_{g1} and NO, but any reasonable assumptions still result in estimates smaller than the X-ray distance of ∼3 Å. For example, assuming (ρ_{Fe}, ρ_N, ρ_O) = (−0.2, 0.75, 0.45), close to the DFT prediction for the −SCH_3-coordinated ferrous−NO heme center,[34] one can estimate R_{NgN} from 2.55 Å (for $\theta_N \approx 90°$) to 3.4 Å (for $\theta_N \approx 0°$; the distance between N_{g1} and $O_{(NO)}$ is ∼2.25 Å).

Similar estimates for spin density distributions with larger ρ_{Fe} return shorter distances. For example, (ρ_{Fe}, ρ_N, ρ_O) = (0.6, 0.25, 0.15)[49] results in R_{NgN} ranging from 1.9 Å ($\theta_N \approx 90°$) to 2.7 Å ($\theta_N \approx 0°$; the distance between N_{g1} and $O_{(NO)} \approx$ 1.55 Å). The distances between N_{g1} and the nearest atom of the NO ligand thus become comparable with the covalent bond length, which makes the spin density distributions with large ρ_{Fe} not realistic. Summarizing the above considerations, we can conclude that, regardless of our assumptions about the spin density distribution in the Fe−N−O fragment (within reasonable limits), the estimated distance between N_{g1} and the nearest atom of the NO ligand is shorter than 2.6 Å.

The fact that the two heme sites were found to have different orientations of the NO ligand in a single crystal sample[38] creates a definite possibility that some sort of the orientational distribution of the NO ligand may also be present in the frozen solutions. Taking into account the relationship between the orientation of the NO ligand and that of the g-tensor axes, one can deduce that the rotation of the NO ligand about the heme plane normal by angle θ_{NO} is equivalent to the rotation of the positions of the nuclei of the molecular surroundings (excluding NO) about the heme normal, with respect to the fixed g-frame. The heme plane normal, which is the rotation axis, lies in the (g_X, g_Y) plane, at the azimuthal angle $\varphi \approx 40°$. Depending on (i) the angular variation in the orientation of the NO ligand, (ii) the angle between the *hfi* axis of a given nucleus and the heme plane normal, and (iii) the EPR position, for which the ENDOR spectrum was recorded, the spectral lines of a given nucleus may be broadened and show extra singularities that would be absent without the rotational distribution. Given this complication and the number of contributing nuclei, it is difficult to obtain a good overall fit to the orientation dependent spectra with reasonable efforts. Therefore, we did not undertake such simulations in this work. Our simulations of

dx.doi.org/10.1021/jp302319c | J. Phys. Chem. A 2012, 116, 6731−6739

FI ENDOR spectra, however, were based on a relatively weak requirement that the anisotropic *hfi* as a function of the NO orientation remains approximately constant, which is supported by the data presented in Table 1.

Since the position of the L-Arg substrate in the frozen solution of EPR sample is different from that in the crystal structure (see above), the H-bonding situation could also be different. Therefore, the lack of the hydrogen bond between the NO ligand and the guanidino nitrogen of Arg for the solution samples of nNOS represents a nontrivial finding. This observation is consistent with the previous reports that it is not the L-Arg substrate itself that would most likely serve as a direct proton donor to the diatomic ligands (NO and O_2) bound to the heme.[38] Emerging evidence indicates that the two NOS reaction steps are distinguished by the substrate-controlled delivery of protons to the ferric−peroxo species, and the H-bonding network appears to be different among the NOS isoforms.[10,12,57-60] Therefore, it is also important to conduct pulsed EPR studies of the Fe(II)−NO complexes in the presence of NOHA (substrate for the second NOS reaction step) as well as samples of other NOS isoforms. Such studies are in progress and should advance our understanding of the NOS enzyme reaction mechanisms and specifically the role of hydrogen bonding.

CONCLUSIONS

In this work, we have studied the location and geometry of the L-Arg substrate at the NO-coordinated ferrous heme center(s) of nNOS by pulsed ENDOR. We have found that, in frozen solutions, the L-Arg location at the heme active site(s) of nNOS is noticeably different from that in single crystals, with the nearby guanidino nitrogen being some 0.5 Å closer to, and the nearby H_δ about 1 Å further from the NO ligand than in the X-ray crystal structure. In spite of its closer position, N_{g1} still does not form a hydrogen bond with the NO ligand, as evidenced by the absence of a significant isotropic *hfi* constant for this nitrogen. This is probably because the geometry for the potential H-bond is not optimal.

The difference between the L-Arg positions obtained in this work (frozen solution) and by X-ray crystallography[38] is most likely related to the structural constraints imposed on the protein by the crystal. The resulting difference between the solution and crystal structures is subtle and only amounts to minor changes of relative positions of various molecular moieties. This assumption is indirectly supported by slight structural rearrangements in the second coordination sphere of the heme center of NOS observed for different types of crystals.[61] The scale of these rearrangements (about 1 Å) is similar to that observed in this work.

The 90° difference between the orientations of the NO ligand observed by X-ray for the two heme sites of nNOS creates a possibility that some sort of the orientational distribution might also exist in the frozen solutions. For this reason, we did not attempt to simulate the orientation-selective ENDOR spectra. The analysis of the field-integrated spectra, however, has resulted in distance estimates for the closest guanidino nitrogen and the nearby proton (deuteron) at C_δ. This work demonstrated the sensitivity of pulsed EPR for studying the geometry of the substrate molecule at the Fe(II)−NO center of NOS.

AUTHOR INFORMATION

Corresponding Author

*Phone: 505-925-4326. Fax: 505-925-4549. E-mail: cfeng@unm.edu.

Notes

The authors declare no competing financial interest.

ACKNOWLEDGMENTS

We thank Professor Brian Crane and Dr. Jawahar Sudhamsu at Cornell University, Professor Nicolai Lehnert at University of Michigan, and Dr. Huiying Li at University of California, Irvine, for helpful discussions. This work was supported by grants from the National Institutes of Health (GM081811 to C.F.; 1S10RR26416-01 to A.V.A), AHA Grant-in-Aid (09GRNT2220310 to C.F.), and NSERC Discovery Grant (183521 to J.G.G.). This project was also supported by grants from the National Center for Research Resources (5P20RR016480-12) and the National Institute of General Medical Sciences (8 P20 GM103451-12). C.F. acknowledges the support of UNM HSC RAC grant.

REFERENCES

(1) Roman, L. J.; Martasek, P.; Masters, B. S. S. *Chem. Rev.* **2002**, *102*, 1179−1189.
(2) Alderton, W. K.; Cooper, C. E.; Knowles, R. G. *Biochem. J.* **2001**, *357*, 593−615.
(3) Abu-Soud, H. M.; Yoho, L. L.; Stuehr, D. J. *J. Biol. Chem.* **1994**, *269*, 32047−32050.
(4) Abu-Soud, H. M.; Stuehr, D. J. *Proc. Natl. Acad. Sci. U.S.A.* **1993**, *90*, 10769−10772.
(5) Panda, K.; Ghosh, S.; Stuehr, D. J. *J. Biol. Chem.* **2001**, *276*, 23349−23356.
(6) Zhu, Y.; Silverman, R. B. *Biochemistry* **2008**, *47*, 2231−2243.
(7) Crane, B. R.; Arvai, A. S.; Ghosh, D. K.; Wu, C. Q.; Getzoff, E. D.; Stuehr, D. J.; Tainer, J. A. *Science* **1998**, *279*, 2121−2126.
(8) Santolini, J. *J. Inorg. Biochem.* **2011**, *105*, 127−141.
(9) Daff, S. *Nitric Oxide* **2010**, *23*, 1−11.
(10) Davydov, R.; Sudhamsu, J.; Lees, N. S.; Crane, B. R.; Hoffman, B. M. *J. Am. Chem. Soc.* **2009**, *131*, 14493−14507.
(11) Woodward, J. J.; Nejaty-Jahromy, Y.; Britt, R. D.; Marletta, M. A. *J. Am. Chem. Soc.* **2010**, *132*, 5105−5113.
(12) Li, D.; Kabir, M.; Stuehr, D. J.; Rousseau, D. L.; Yeh, S. R. *J. Am. Chem. Soc.* **2007**, *129*, 6943−6951.
(13) Raman, C. S.; Li, H. Y.; Martasek, P.; Kral, V.; Masters, B. S. S.; Poulos, T. L. *Cell* **1998**, *95*, 939−950.
(14) Li, H. Y.; Shimizu, H.; Flinspach, M.; Jamal, J.; Yang, W. P.; Xian, M.; Cai, T. W.; Wen, E. Z.; Jia, Q. A.; Wang, P. G.; Poulos, T. L. *Biochemistry* **2002**, *41*, 13868−13875.
(15) Garcin, E. D.; Arvai, A. S.; Rosenfeld, R. J.; Kroeger, M. D.; Crane, B. R.; Andersson, G.; Andrews, G.; Hamley, P. J.; Mallinder, P. R.; Nicholls, D. J.; St-Gallay, S. A.; Tinker, A. C.; Gensmantel, N. P.; Mete, A.; Cheshire, D. R.; Connolly, S.; Stuehr, D. J.; Aberg, A.; Wallace, A. V.; Tainer, J. A.; Getzoff, E. D. *Nat. Chem. Biol.* **2008**, *4*, 700−707.
(16) Zhang, J.; Martasek, P.; Paschke, R.; Shea, T.; Masters, B. S. S.; Kim, J. J. P. *J. Biol. Chem.* **2001**, *276*, 37506−37513.
(17) Garcin, E. D.; Bruns, C. M.; Lloyd, S. J.; Hosfield, D. J.; Tiso, M.; Gachhui, R.; Stuehr, D. J.; Tainer, J. A.; Getzoff, E. D. *J. Biol. Chem.* **2004**, *279*, 37918−37927.
(18) Xia, C.; Misra, I.; Iyanagi, T.; Kim, J.-J. P. *J. Biol. Chem.* **2009**, *284*, 30708−30717.
(19) Aoyagi, M.; Arvai, A. S.; Tainer, J. A.; Getzoff, E. D. *EMBO J.* **2003**, *22*, 766−775.
(20) Ghosh, D. K.; Abu-Soud, H. M.; Stuehr, D. J. *Biochemistry* **1995**, *34*, 11316−11320.

(21) Sheta, E. A.; McMillan, K.; Masters, B. S. S. *J. Biol. Chem.* **1994**, *269*, 15147−15153.
(22) Feng, C. *Coord. Chem. Rev.* **2012**, *256*, 393−411.
(23) Ilagan, R. P.; Tejero, J. S.; Aulak, K. S.; Ray, S. S.; Hemann, C.; Wang, Z.-Q.; Gangoda, M.; Zweier, J. L.; Stuehr, D. J. *Biochemistry* **2009**, *48*, 3864−3876.
(24) Feng, C. J.; Tollin, G.; Holliday, M. A.; Thomas, C.; Salerno, J. C.; Enemark, J. H.; Ghosh, D. K. *Biochemistry* **2006**, *45*, 6354−6362.
(25) Feng, C. J.; Thomas, C.; Holliday, M. A.; Tollin, G.; Salerno, J. C.; Ghosh, D. K.; Enemark, J. H. *J. Am. Chem. Soc.* **2006**, *128*, 3808−3811.
(26) Astashkin, A. V.; Elmore, B. O.; Fan, W.; Guillemette, J. G.; Feng, C. *J. Am. Chem. Soc.* **2010**, *132*, 12059−12067.
(27) Galli, C.; MacArthur, R.; Abu-Soud, H. M.; Clark, P.; Stuehr, D. J.; Brudvig, G. W. *Biochemistry* **1996**, *35*, 2804−2810.
(28) Astashkin, A. V.; Fan, W.; Elmore, B. O.; Guillemette, J. G.; Feng, C. *J. Phys. Chem. A* **2011**, *115*, 10345−10352.
(29) Davydov, R.; Ledbetter-Rogers, A.; Martasek, P.; Larukhin, M.; Sono, M.; Dawson, J. H.; Masters, B. S. S.; Hoffman, B. M. *Biochemistry* **2002**, *41*, 10375−10381.
(30) Stoll, S.; Nejaty-Jahromy, Y.; Woodward, J. J.; Ozarowski, A.; Marletta, M. A.; Britt, R. D. *J. Am. Chem. Soc.* **2010**, *132*, 11812−11823.
(31) Tierney, D. L.; Martasek, P.; Doan, P. E.; Masters, B. S. S.; Hoffman, B. M. *J. Am. Chem. Soc.* **1998**, *120*, 2983−2984.
(32) Tierney, D. L.; Huang, H.; Martasek, P.; Roman, L. J.; Silverman, R. B.; Masters, B. S. S.; Hoffman, B. M. *J. Am. Chem. Soc.* **2000**, *122*, 5405−5406.
(33) Praneeth, V. K. K.; Neese, F.; Lehnert, N. *Inorg. Chem.* **2005**, *44*, 2570−2572.
(34) Praneeth, V. K. K.; Haupt, E.; Lehnert, N. *J. Inorg. Biochem.* **2005**, *99*, 940−948.
(35) Praneeth, V. K. K.; Näther, C.; Peters, G.; Lehnert, N. *Inorg. Chem.* **2006**, *45*, 2795−2811.
(36) The spin populations of N and O predicted by DFT are about 0.5 and 0.3, respectively: Lehnert, N., private communication.
(37) Stuehr, D. J.; Santolini, J.; Wang, Z. Q.; Wei, C. C.; Adak, S. *J. Biol. Chem.* **2004**, *279*, 36167−36170.
(38) Li, H. Y.; Igarashi, J.; Jamal, J.; Yang, W. P.; Poulos, T. L. *J. Biol. Inorg. Chem.* **2006**, *11*, 753−768.
(39) Feng, C. J.; Tollin, G.; Hazzard, J. T.; Nahm, N. J.; Guillemette, J. G.; Salerno, J. C.; Ghosh, D. K. *J. Am. Chem. Soc.* **2007**, *129*, 5621−5629.
(40) Ghosh, D. K.; Holliday, M. A.; Thomas, C.; Weinberg, J. B.; Smith, S. M. E.; Salerno, J. C. *J. Biol. Chem.* **2006**, *281*, 14173−14183.
(41) Ghosh, D. K.; Wu, C. Q.; Pitters, E.; Moloney, M.; Werner, E. R.; Mayer, B.; Stuehr, D. J. *Biochemistry* **1997**, *36*, 10609−10619.
(42) Astashkin, A. V.; Enemark, J. H.; Raitsimring, A. *Concepts Magn. Reson., Part B* **2006**, *29B*, 125−136.
(43) Patchkovskii, S.; Ziegler, T. *Inorg. Chem.* **2000**, *39*, 5354−5364.
(44) Migita, C. T.; Salerno, J. C.; Masters, B. S. S.; Martasek, P.; McMillan, K.; Ikeda-Saito, M. *Biochemistry* **1997**, *36*, 10987−10992.
(45) O'Keeffe, D. H.; Ebel, R. E.; Peterson, J. A. *J. Biol. Chem.* **1978**, *253*, 3509−3516.
(46) Shiro, Y.; Fujii, M.; Isogai, Y.; Adachi, S.-I.; Iizuka, T.; Obayashi, E.; Makino, R.; Nakahara, K.; Shoun, H. *Biochemistry* **1995**, *34*, 9052−9058.
(47) Karthein, R.; Nastainczyk, W.; Ruf, H. H. *Eur. J. Biochem.* **1987**, *166*, 173−180.
(48) Hori, H.; Ikeda-Saito, M.; Yonetani, T. *J. Biol. Chem.* **1981**, *256*, 7849−7855.
(49) Radoul, M.; Bykov, D.; Rinaldo, S.; Cutruzzolà, F.; Neese, F.; Goldfarb, D. *J. Am. Chem. Soc.* **2011**, *133*, 3043−3055.
(50) Astashkin, A. V.; Klein, E. L.; Enemark, J. H. *J. Inorg. Biochem.* **2007**, *101*, 1623−1629.
(51) Astashkin, A. V.; Johnson-Winters, K.; Klein, E. L.; Byrne, R. S.; Hille, R.; Raitsimring, A. M.; Enemark, J. H. *J. Am. Chem. Soc.* **2007**, *129*, 14800−14810.
(52) Olympia, P. L., Jr.; Wei, I. Y.; Fung, B. M. *J. Chem. Phys.* **1969**, *51*, 1610−1614.
(53) Semin, G. K.; Babushkina, T. A.; Yakobson, G. G. *Nuclear Quadrupole Resonance in Chemistry*; John Willey and Sons: New York, 1975.
(54) Astashkin, A. V.; Kawamori, A.; Kodera, Y.; Kuroiwa, S.; Akabori, K. *J. Chem. Phys.* **1995**, *102*, 5583−5588.
(55) Astashkin, A. V.; Hara, H.; Kuroiwa, S.; Kawamori, A.; Akabori, K. *J. Chem. Phys.* **1998**, *108*, 10143−10151.
(56) Lin, T.-J.; O'Malley, P. J. *J. Phys. Chem. B* **2011**, *115*, 4227−4233.
(57) Crane, B. R.; Sudhamsu, J.; Patel, B. A. *Annu. Rev. Biochem.* **2010**, *79*, 445−470.
(58) Pant, K.; Crane, B. R. *Biochemistry* **2006**, *45*, 2537−2544.
(59) Papale, D.; Bruckmann, C.; Gazur, B.; Miles, C. S.; Mowat, C. G.; Daff, S. *Biochem. J.* **2012**, *443*, 505−514.
(60) Giroud, C.; Moreau, M.; Mattioli, T. A.; Balland, V.; Boucher, J.-L.; Xu-Li, Y.; Stuehr, D. J.; Santolini, J. *J. Biol. Chem.* **2010**, *285*, 7233−7245.
(61) Crane, B. R.; Arvai, A. S.; Gachhui, R.; Wu, C. Q.; Ghosh, D. K.; Getzoff, E. D.; Stuehr, D. J.; Tainer, J. A. *Science* **1997**, *278*, 425−431.